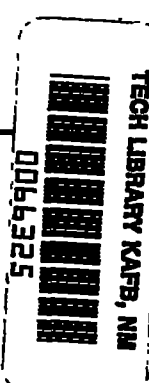


NACA TN 3707 \$2.00



NATIONAL ADVISORY COMMITTEE FOR AERONAUTICS

TECHNICAL NOTE 3707

FLUTTER OF THIN PROPELLER BLADES, INCLUDING EFFECTS
OF MACH NUMBER, STRUCTURAL DAMPING, AND
VIBRATORY-STRESS MEASUREMENTS NEAR
THE FLUTTER BOUNDARIES

By Harvey H. Hubbard, Marvin F. Burgess,
and Maurice A. Sylvester

Langley Aeronautical Laboratory
Langley Field, Va.



Washington

June 1956

APR 1956
U.S. GOVERNMENT PRINTING OFFICE: 1956 7-1200



0066325

TECHNICAL NOTE 3707

FLUTTER OF THIN PROPELLER BLADES, INCLUDING EFFECTS
OF MACH NUMBER, STRUCTURAL DAMPING, AND
VIBRATORY-STRESS MEASUREMENTS NEAR
THE FLUTTER BOUNDARIES

By Harvey H. Hubbard, Marvin F. Burgess,
and Maurice A. Sylvester

SUMMARY

Experimental results are presented of an investigation on the flutter of propeller blades with three different plan forms. Data for a proposed supersonic propeller having highly twisted 2-percent-thick blades indicate that the flutter boundaries are complex and that several modes of flutter are involved. Data for a 6-percent-thick blade for which both the high Mach number and the low Mach number flutter boundaries are obtained in detail indicate that Mach number effects can be beneficial in alleviating flutter. Results for two 3-percent-thick blades having different internal damping show that an increase in the internal damping is beneficial in reducing the magnitude of the stresses both during flutter and for conditions of blade resonance.

INTRODUCTION

Stall flutter is recognized as one of the most serious vibration problems encountered in propeller and compressor operation. Although a large amount of information is available from full-scale tests over a period of time from World War I to the present, these data are difficult to correlate because of the wide variations of the test conditions. A few systematic studies are available in which attempts were made to isolate the effects of some of the significant parameters in the problem. Reference 1, in particular, contains data on the effects of torsional stiffness, section thickness ratio, sweepback, length-chord ratio, section center-of-gravity location, blade twist, blade taper, Mach number, and fluid density. A criterion is also presented in reference 1 which stipulates the conditions necessary for flutter-free operation of propeller blades.

The present paper contains results of an investigation on the flutter of propeller blades with three different plan forms. Some of the data were obtained in the same manner as those of reference 1 and are extensions of that work. Specific attention was given to tests of a suggested supersonic propeller having highly twisted 2-percent-thick blades. This model was operated over a typical blade-angle range in order to define its boundaries for torsion, bending, and bending-torsion modes of flutter. Tests were also made with a 6-percent-thick propeller in which the speed of sound of the medium was changed in order to study the shape of the flutter boundaries, particularly for the higher Mach numbers of operation. In addition, some effects of structural damping on the flutter boundaries as well as on the blade stresses during operation near the flutter boundary were studied for an untwisted 3-percent-thick propeller.

SYMBOLS

a	speed of sound in operating medium, ft/sec
b	blade semichord, ft
$b\omega_a/a$	sound-speed coefficient
D	blade diameter, ft
EI	bending stiffness, lb-ft ²
f	frequency of recorded oscillation, cps
f_{h1}	natural first bending frequency, cps
f_{h2}	natural second bending frequency, cps
f_n	natural frequency at propeller rotational speed, cps
$f_{n=0}$	natural frequency at zero rotational speed, cps
f_a	natural torsional frequency, cps
g_a	torsional damping coefficient
g_h	bending damping coefficient
GJ	torsional stiffness, lb-ft ²

h	blade thickness, ft
I_{cg}	polar moment of inertia about section center-of-gravity location per unit length, slug-ft ² /ft
K	Southwell coefficient
l	blade length, ft
M	Mach number
m	blade mass per unit length, slugs/ft
n	propeller rotational speed, rps
r_{cg}	nondimensional radius of gyration of blade section about section center-of-gravity location, $\sqrt{I_{cg}/mb^2}$
v	blade velocity, ft/sec
$V/b\alpha_a$	flutter-speed coefficient
β	blade angle, deg
μ	relative-density factor
ρ	mass density of operating medium, slugs/cu ft
ω_a	natural torsional circular frequency, radians/sec

Subscript:

0.87 referred to 0.8-blade-length station

APPARATUS**Test Facility**

Tests were conducted in the Langley vacuum sphere, previously described in reference 1, in which both the speed of sound and the pressure of the medium were varied. Pressures ranging from 1/6 atmosphere to full atmosphere were used in the present tests. Mixtures of Freon-12 and air were used in various proportions to give speeds of sound from approximately 550 to 1,100 feet per second. A 500-horsepower variable-speed electric motor was used to drive the propeller models which were tested at zero advance except for the induced flow.

Modal Blades and Hubs

The plan forms of the four model blades tested are shown in figure 1 and additional information about the physical characteristics of each blade is given in table I. These models were all tested as one-blade configurations with suitable counterweights attached as in reference 1.

Model 1 (model of proposed steel supersonic propeller) was a twisted blade with NACA 16-series symmetrical airfoil sections and was of solid aluminum-alloy construction. It was tested in a fixed-pitch hub for the purpose of defining the flutter regions for an extremely thin (2-percent-thick) blade. Blade-plan-form curves for this model are given in figure 2.

Model 2 had an NACA 16-006 airfoil section, was untwisted, and was of solid aluminum-alloy construction. This blade was tested in both the fixed- and controllable-pitch hubs for comparison. Most of the testing was done with the controllable-pitch hub for the purpose of more carefully determining the boundaries of the flutter regions, particularly the upper boundaries.

Models 3a and 3b were identical in plan form and differed only in the method of construction. They were untwisted and had NACA 16-003 airfoil sections. Model 3a was solid steel whereas model 3b consisted of two laminations of steel bonded together flatwise with Cycleweld cement. The objective in laminating model 3b was to introduce additional internal blade damping in the same manner as described in reference 2. Both of these models were tested in a fixed-pitch hub.

Instrumentation

Bending and torsion strains near the root of the blade were obtained by means of strain gages located as shown in figure 1. Oscillograph recordings were made from which frequencies of oscillation were determined. The rotational speed, which for zero forward velocity is equivalent to the resultant velocity, was recorded on the same record. Blade angles were measured while the propeller was at rest in all cases. Twist angles were measured optically with the aid of stroboscopic light during the tests of model 1 and have been included in the presentation of the data as an aid in the interpretation of the test results.

TEST PROCEDURES

The same general procedures were used in the present tests as for the tests of reference 1. At a given atmospheric pressure and blade angle, runs were made at various rotational speeds until flutter was

obtained. Results of several runs at different blade angles were useful in defining the flutter boundaries. For some cases in which a controllable-pitch hub was used, both blade angle and rotational speed were varied during the run to expedite the definition of certain portions of the flutter boundary.

Flutter speed, as defined in this paper, is the lowest speed at which a sustained oscillation in either bending or torsion was detected. In some instances for models 3a and 3b where flutter was not severe, the flutter speed was exceeded in order to obtain stress data inside the flutter boundary. It was also possible, in some cases, to pass through a given flutter region and to define other flutter regions at higher speeds.

Damping values as listed in the paper were determined from the decrements of strain-gage signals recorded while the blades were mounted in the hubs, which were in all cases mounted on the motor shaft, but not rotating.

RESULTS AND DISCUSSION

The results of flutter tests on the propeller models listed in table I are discussed under two headings. The effects of such parameters as thickness, built-in twist, Mach number, and structural damping on the shape of the flutter boundaries are first discussed. These data are presented conventionally in the form of flutter-speed coefficients as a function of blade angle. Some discussion is then given to the bending and torsional stresses measured in the vicinity of the stall flutter boundary for two models differing in their amounts of internal blade damping.

Effects of Various Parameters on the Stall

Flutter Boundaries

Thickness and built-in twist.- The results of the flutter tests on model 1 are presented in figure 3. Data are plotted in the form of flutter-speed coefficients as a function of blade angle (which, as explained later, includes blade twist) for density values of the operating medium of 0.00079 and 0.00040 slug/cu ft. In the term $(V/b\omega_a)_{0.8l}$, V is the velocity of the propeller blade at the 0.8-blade-length station, b is the semichord at that station, and ω_a is the blade natural torsional circular frequency. Also noted in the figure are the flutter frequencies which can be compared with the rotational frequencies of the right-hand vertical scale. In general, the recorded frequencies of the data plotted in figure 3 are not integral multiples of the rotational speed.

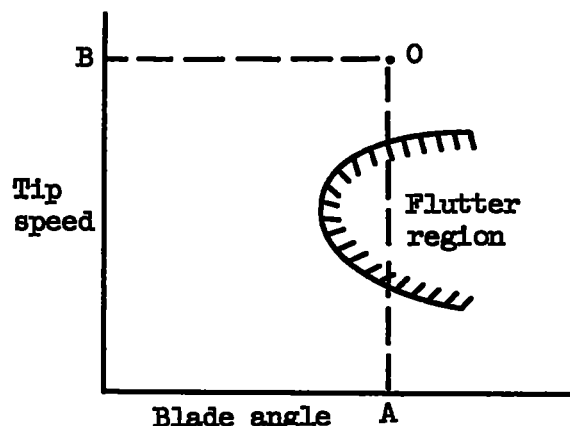
Model 1 was tested at reduced pressure to make the present test conditions comparable to the operating conditions of the proposed full-scale propeller. During these tests, the model was operated over a wide blade-angle range in order to define its flutter boundary. Because this blade was only 2 percent thick and because of a fairly large amount of built-in twist, particular attention was given to a determination of the amount of twist-up encountered during testing. The twist angles were measured optically for the 0.8-blade-length station and have been indicated by the lines of long dashes in figure 3 as an aid in the interpretation of the data. The forces on the blade tending to twist it result from the following components: (1) the aerodynamic pitching moments, (2) the chordwise components of the centrifugal forces (ref. 3), and (3) the radial components of the centrifugal forces tending to straighten the blade (ref. 4). All these effects are additive in the negative blade-angle range and, hence, the amount of twist-up is large. For positive blade angles, components (2) and (3) oppose each other and, hence, the amount of twist-up is less.

The tests were conducted by initially setting a given blade angle and then increasing the speed until flutter was encountered. The long-dashed lines in figure 3 are in a sense operating lines since they indicate the actual blade angle as measured during the run at various speeds as opposed to the static blade angle measured at the start of the run. In some cases, it was possible to pass completely through one or more flutter regions before the sustained oscillations became sufficiently violent to curtail the testing. As indicated in the figure, three types of flutter were obtained for this model. In general, torsional oscillations and coupled bending-torsion oscillations were associated with milder flutter than the bending oscillations. As a matter of interest, the blade failed while operating near the bending flutter boundary.

The data of figure 3(a) indicate that it would be very difficult to schedule the operation of this propeller in such a manner as to avoid these flutter regions. At a lower ambient pressure, however, as in figure 3(b), the flutter boundaries are somewhat different and it appears that the propeller could be increased in speed without encountering flutter, provided the blade angle were changed with speed to avoid the flutter regions. The bending flutter region was eliminated entirely in the range of these tests, and the bending-torsion flutter region was greatly reduced in extent. The torsional oscillations encountered were also mild for the range of blade angles tested and were safely traversed. No attempt was made at this value of the density to evaluate the minimum flutter-speed coefficient which would normally be associated with the higher positive blade angles.

Mach number.-- There was some indication in the work of reference 1 that the flutter regions of propellers might be limited mainly to the subsonic tip-speed range. Thus, at a given blade angle, if flutter were

not encountered up to a tip speed corresponding to a Mach number of approximately 1.0, no flutter would be encountered at higher tip speeds. This result suggested that the upper extent of the flutter region was limited because of Mach number effects. This phenomenon is illustrated schematically in the following sketch where a hypothetical flutter region having both an upper and a lower boundary is plotted:



If operation of the propeller at point O were desired, a schedule of operation in which the blade angle was first increased to A and then the tip speed was increased to the desired operating point might result in destruction of the blade since part of the flutter region would be traversed. On the other hand if the tip speed were first increased to B, the blade angle could then be safely increased to the desired operating point without encountering flutter. The use of a controllable-pitch hub in these tests of model 2 had the objectives of defining both the upper and lower flutter boundaries and of exploring in more detail the possibility of this type of operating procedure.

The main variable in these tests was the speed of sound of the operating medium. Results are shown in figure 4 in which flutter-speed coefficients are plotted as a function of blade angle for three values of the sound-speed coefficient. Sound-speed coefficient is defined as $(b\omega_a/a)_{0.8l}$, where b is the blade semichord at the 0.8-blade-length station, ω_a is the first torsional circular frequency of the blade, and a is the speed of sound of the operating medium. At the lowest value of the sound-speed coefficient, which incidentally corresponds to the full atmospheric density in air for this model, only the lower portion of the flutter boundary was defined because of stress limitations. In general, it can be seen that the flutter region becomes smaller as the sound-speed coefficient becomes larger. The trend of figure 4 indicates that there would be no flutter region at all at a value slightly higher than 0.51. This trend is a confirmation of the findings of reference 1 and appears to be a Mach number effect.

The data of figure 4 are replotted in figure 5 to show this effect more directly as a function of Mach number. The Mach number at flutter is plotted as a function of blade angle for three values of the sound-speed coefficient. It can be seen that flutter occurs over a smaller blade-angle range at the higher Mach numbers. At a sufficiently high Mach number, safe operation of this propeller above the flutter boundary is possible. The Mach number was first increased at low blade angles and then the blade angle was increased to higher values while Mach number remained constant. In a few cases, it was then possible to reduce Mach number for the purpose of defining the upper flutter boundary. For this particular propeller, the classical-flutter speed was either higher than could be obtained in the tests or did not exist at all for these conditions.

Structural damping.- Increasing the structural damping has been suggested as a way of increasing the minimum stall flutter speed of propeller blades. One method that suggests itself is to add damping at the root of the blade. Another method is the addition of damping in the blade itself as has been suggested in reference 2. Some attempt has been made to vary both the blade and hub damping during the present tests and the results of these tests are discussed in this section.

The effect of hub damping on stall flutter is shown in figure 6 where the flutter-speed coefficient is plotted as a function of blade angle for two values of the torsional damping coefficient. These data are for model 2 tested in full atmospheric density. The structural damping coefficients apply to the hub and blade in combination and were obtained while the blade was not rotating. The difference in the damping is believed to be due to the differences in the hubs since the same blade is used in both cases. The results of figure 6 indicate that increasing the torsional damping coefficient from $g_a = 0.004$ to $g_a = 0.022$ was effective in increasing the minimum flutter-speed coefficient by approximately 40 percent. This result is in conformity with those obtained for the thin wings in reference 5.

In order to study the effect of internal blade damping, models 3a and 3b were fabricated and tested. Model 3a was of solid steel construction and thus had relatively low internal damping. Model 3b was of laminated construction designed to give increased internal damping. The method of construction was the same as for model V of reference 2 inasmuch as that model seemed to give the largest increase in internal damping over the basic configuration.

The values of torsional damping coefficient g_a for each of these two models mounted in a fixed-pitch hub on the motor shaft are given in figure 7 as a function of vibratory torsional stress. The damping in each case is seen to be approximately a linear function of the stress for the range of the tests. For the solid blade, the damping is seen to

vary from approximately 0.0023 to 0.0043, which is of the same order of magnitude as the values obtained in reference 2 during bench tests. The overall damping values are seen to be approximately 50 percent higher for the laminated blade than for the solid blade at comparable stress values. It is believed that this increase over the basic configuration is an indication of the change in the blade damping since both models were tested in the same hub arrangement. This increase in damping is much less than had been anticipated on the basis of results in reference 2.

The effects on the flutter boundaries of the additional damping obtained with model 3b are shown in figure 8. The flutter-speed coefficients are plotted as a function of blade angle for two different densities. At full atmospheric density ($\rho = 0.00238$ slug/cu ft), there are no noticeable differences in the flutter boundaries for the range of the tests; however, at 1/4 atmospheric density ($\rho = 0.00059$ slug/cu ft), the blade having the higher damping also had somewhat higher flutter-speed coefficients as indicated in figure 8(b).

Blade Stresses Near the Flutter Boundary

Some stress data were recorded for models 3a and 3b in order to evaluate the effects of the additional internal damping of model 3b. It was noted that in the vicinity of the flutter boundary several resonance conditions were encountered during which rather high stresses were noted. In order to assist in the interpretation of some of the stress data, figure 9 has been prepared to give the frequency spectra of these two model blades.

The frequency spectra shown in figure 9 by the solid lines consist of the first bending, second bending, and first torsional blade frequencies plotted as a function of the rotational speed. Also shown by the dashed lines are the rotational harmonics of order 1 to 9. The values of the blade frequencies at zero rotational speed are measured and are approximately the same for both models. The effects of rotational speed on the first and second bending frequencies were calculated by means of the Southwell relation:

$$(f_n)^2 = (f_{n=0})^2 + Kn^2$$

where K is the Southwell coefficient which depends for its value on the blade geometry, angle of attack, and the mode of vibration. For the calculations of this paper, the values of K for the bending frequencies were determined by extrapolating those presented in reference 6 to the blade-offset values of these tests. The effect of rotational speed on the torsional frequency was estimated from the recorded oscillation frequencies for a blade angle of 24°.

The blade torsional and bending vibratory stresses, respectively, are shown in figures 10 and 11 as a function of rotational speed for models 3a and 3b. Data were obtained for two blade-angle settings near the stall and for air densities of 0.00238 and 0.00059 slug/cu ft. Data shown in the figures are considered representative of those of the tests and allow a comparison of the stresses directly for two blades which have different internal damping but which are otherwise nearly identical. It is also possible from the data presented to note the effects of density of the medium on the measured stresses.

During the tests, several major resonance points were noted for which the torsional stresses were fairly high. The maximum stresses at the rotational speeds of these resonances were recorded and are presented in figure 10. The stresses are generally lower for the blade that has the larger amount of damping (model 3b). As was noted previously the sharp rise in the stresses at flutter was not appreciably retarded at atmospheric density of 0.00238 slug/cu ft as indicated in figures 10(a) and 10(b). At a lower atmospheric density ($\rho = 0.00059$ slug/cu ft), the rise in flutter stresses is delayed somewhat for the blade with additional damping. At the higher density, it was not possible to penetrate the flutter region to any great extent by increasing speed because of this rapid rise in the stresses. At the lower density, however, it was possible to penetrate a considerable distance into the flutter region before limiting stresses were reached. As a matter of interest, for the conditions of figure 10(d), it is believed that no flutter was obtained although rather high vibratory stresses were recorded at some of the resonances encountered. Although decreasing density has a beneficial effect on the flutter stresses, those stresses measured during resonances are still severe and of the same order of magnitude as the flutter stresses.

These latter data, which illustrate the response of a low-damped system to a periodic forcing function, point up the problem of interpretation of data obtained in such tests. In the case of resonance peaks such as are shown in figure 10(d), the frequency of oscillations tend to be integral multiples of the rotational speed; whereas, in a flutter condition, this is not normally the case. It is thus convenient to have a spectrum plot of the type shown in figure 9 as an aid in interpretation of results.

The vibratory bending stresses, which were obtained at the same time as the vibratory torsional stresses just discussed, are shown in figure 11. Several major resonance points occur also in the bending records. These major responses are found to occur when the natural frequencies of the blades coincide approximately with integral multiples of the propeller rotational speed. In general, the bending stresses tend to be lower than the torsional stresses in this operating range. Also, the flutter mode is primarily a torsional frequency in this operating range since the bending stresses do not clearly define the condition for the onset of

flutter. As in the case of the torsional stresses, the bending stresses generally show a decrease with decreasing density for the speed range of the tests. At the lower density, there is also a tendency for the measured bending stresses to be lower for the blade with the higher damping.

CONCLUSIONS

An investigation relating to the flutter of thin propeller blades with three different plan forms has been conducted and the following results have been obtained:

1. A highly twisted 2-percent-thick blade was observed to have rather complex flutter boundaries and to flutter in bending, torsion, or bending-torsion modes depending on its operating conditions.
2. Both the upper and lower flutter boundaries were defined for a 6-percent-thick blade for which the Mach number effects appeared to limit the extent of the flutter region. This phenomenon made possible flutter-free operation at tip speeds corresponding to a Mach number of approximately 1.0 for all blade angles.
3. Increases in the minimum flutter-speed coefficients were noted for increases in structural damping and, in particular, hub damping.
4. Internal blade damping was shown to be generally beneficial in reducing the magnitude of the vibratory stresses of a 3-percent-thick blade during flutter.
5. At some resonance conditions, stresses of the same order of magnitude as the flutter stresses were encountered. These stresses were also lower for increased internal blade damping.

Langley Aeronautical Laboratory,
National Advisory Committee for Aeronautics,
Langley Field, Va., March 28, 1956.

REFERENCES

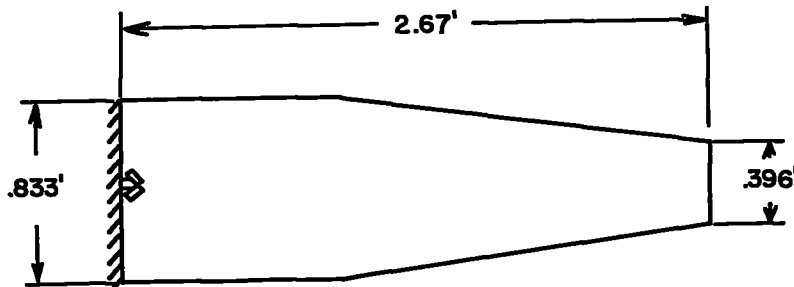
1. Baker, John E.: The Effects of Various Parameters, Including Mach Number, on Propeller-Blade Flutter With Emphasis on Stall Flutter. NACA TN 3357, 1955. (Supersedes NACA RM 150L12b.)
2. Heath, Atwood R., Jr.: Some Torsional-Damping Measurements of Laminated Beams As Applied to the Propeller Stall-Flutter Problem. NACA RM 153A19, 1953.
3. Sterne, L. H. G.: The Structural Aspects of Propeller Design. Rep. No. Structures 5, British R.A.E., July 1947.
4. Biot, M. A.: Increase of Torsional Stiffness of a Prismatical Bar Due to Axial Tension. Jour. Appl. Phys., vol. 10, no. 12, Dec. 1939, pp. 860-864.
5. Rainey, A. Gerald: Preliminary Study of Some Factors Which Affect the Stall-Flutter Characteristics of Thin Wings. NACA TN 3622, 1956. (Supersedes NACA RM 152D08.)
6. Intema, Robert T.: Simplified Procedures and Charts for the Rapid Estimation of Bending Frequencies of Rotating Beams. NACA TN 3459, 1955. (Supersedes NACA RM 154G02.)

TABLE I
DESCRIPTION OF PROPELLER-FIPLATE MODELS

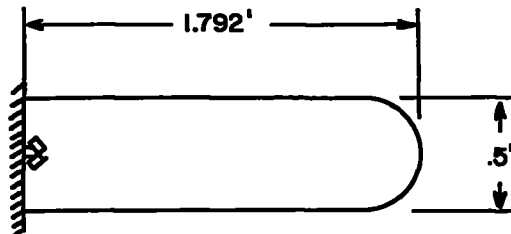
Model	NACA airfoil section	Blade material	$b_{0.87}$, ft	l , ft	r_{hl} , cps	r_{h2} , cps	r_{cl} , cps	Center-of-gravity location, percent chord	Elastic-axis location, percent chord	$\mu_{0.81}$	r_{cg}^2	a_h	a_d	GJ , lb-ft ²	M , lb-ft ²
1	16-series symmetrical	Aluminum alloy	0.265	2.67	8.8	28.0	184.0	48.2	—	41	—	—	—	—	—
2	16-006	Aluminum alloy	.25	1.792	20.0	134.0	185.0	48.5	44.0	127	0.250	0.011, (0.058)	0.004, (0.022)	1,400	882
3a	16-003	Steel	.25	1.773	11.27	69.0	95.3	48.3	50.0	182	.227	.001 to .003	.003 to .005	521	353
3b	16-003	Laminated steel	.25	1.773	11.4	70.0	96.5	48.2	49.8	174	.229	.002 to .005	.004 to .006	511	365

* $\mu_{0.81}$ computed for $\rho = 0.00258$ slug/cu ft.

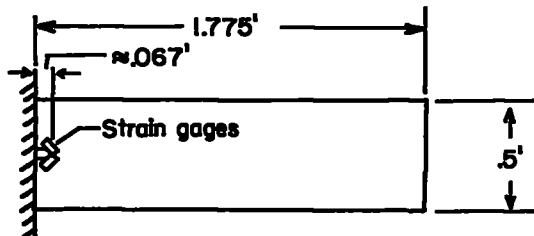
** Values of damping given in parentheses were obtained in controllable-pitch hub and values not in parentheses were obtained in fixed-pitch hub; where a range of values are given, the low values are for low amplitudes and the high values are for high amplitudes.



(a) Model 1 (model of proposed supersonic propeller). Hub radius, 1.25 feet; blade thickness, 2 percent; twisted 31° from root to tip (see fig. 2).



(b) Model 2 used for Mach number studies. Hub radius, 1.27 feet; blade thickness, 6 percent; zero twist.



(c) Models 3a and 3b used for structural damping and stress studies. Hub radius, 1.225 feet; blade thickness, 3 percent; zero twist.

Figure 1.- Propeller flutter-test blades.

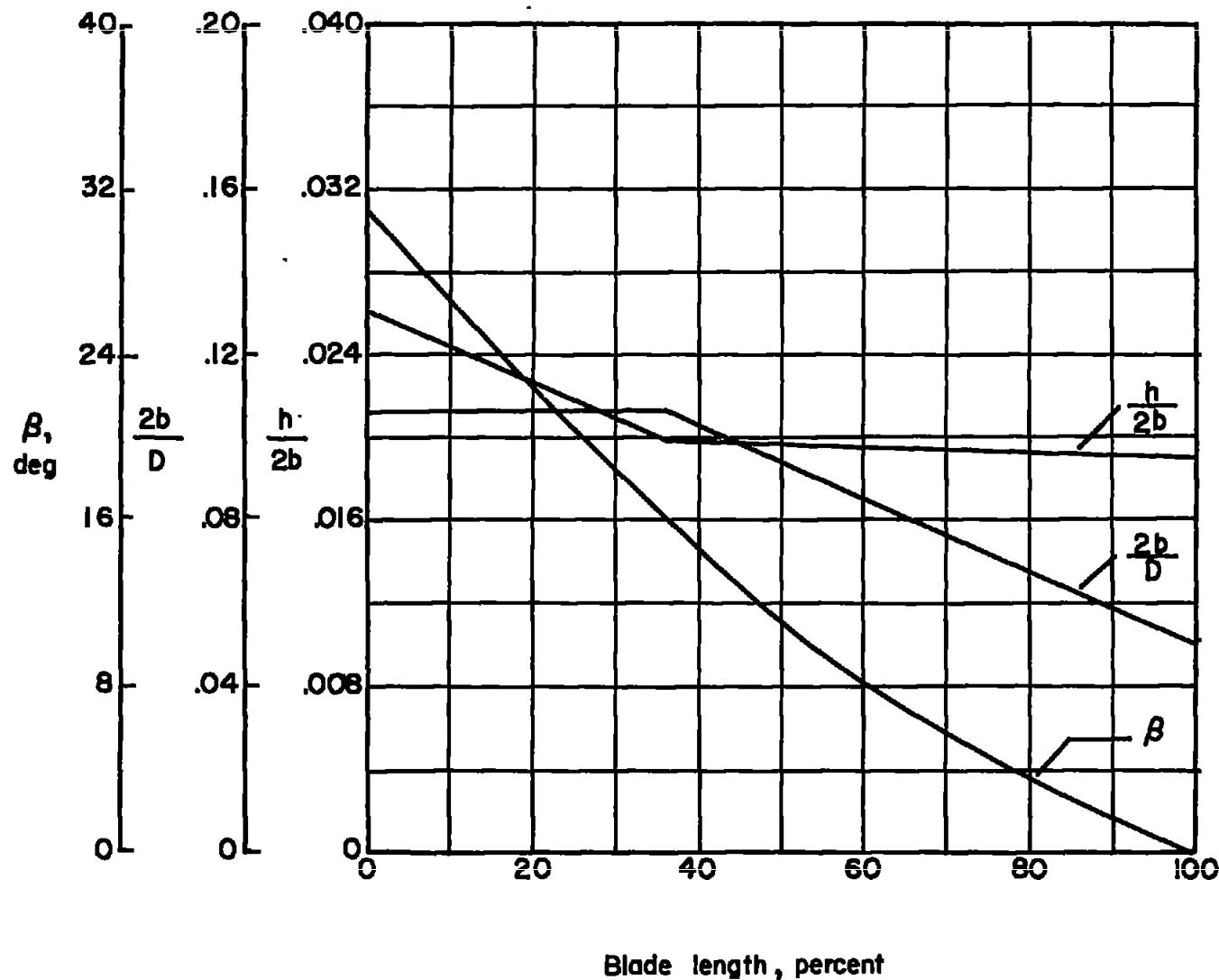


Figure 2.- Blade-plan-form curves for model 1.

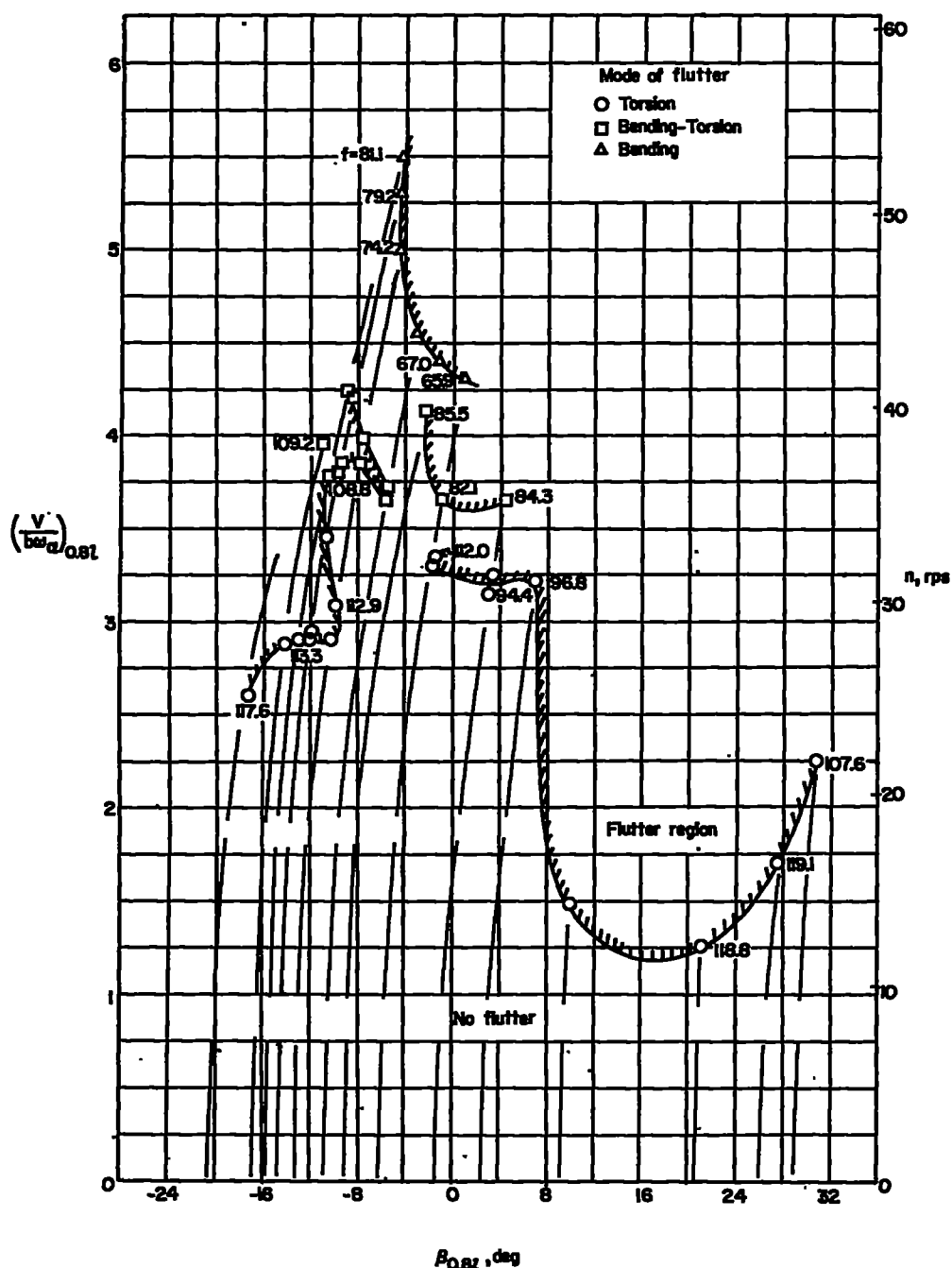
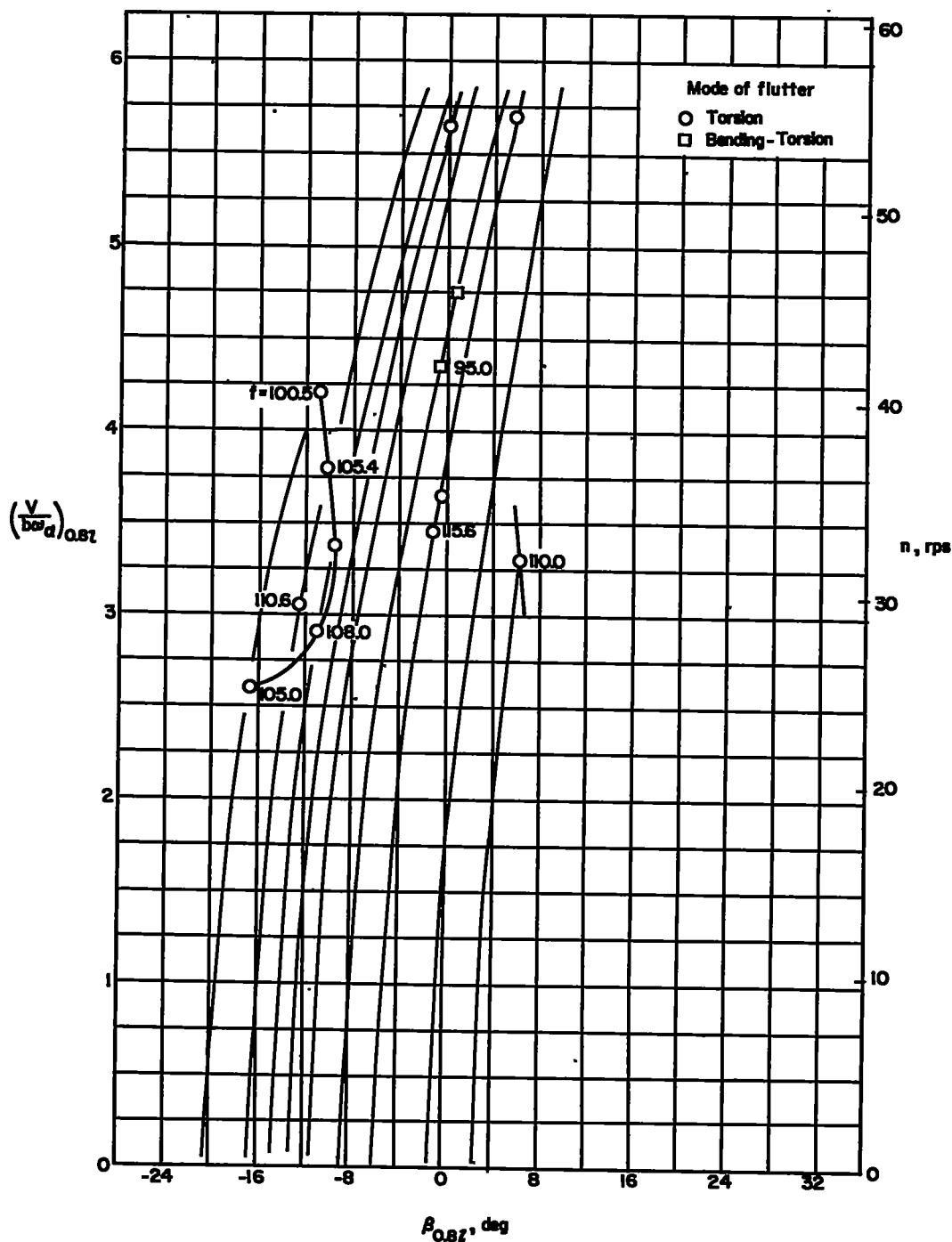
(a) $\rho = 0.00079 \text{ slug/cu ft.}$

Figure 3.- Flutter-speed coefficient as a function of blade angle.
Model 1.



(b) $\rho = 0.00040$ slug/cu ft.

Figure 3.- Concluded.

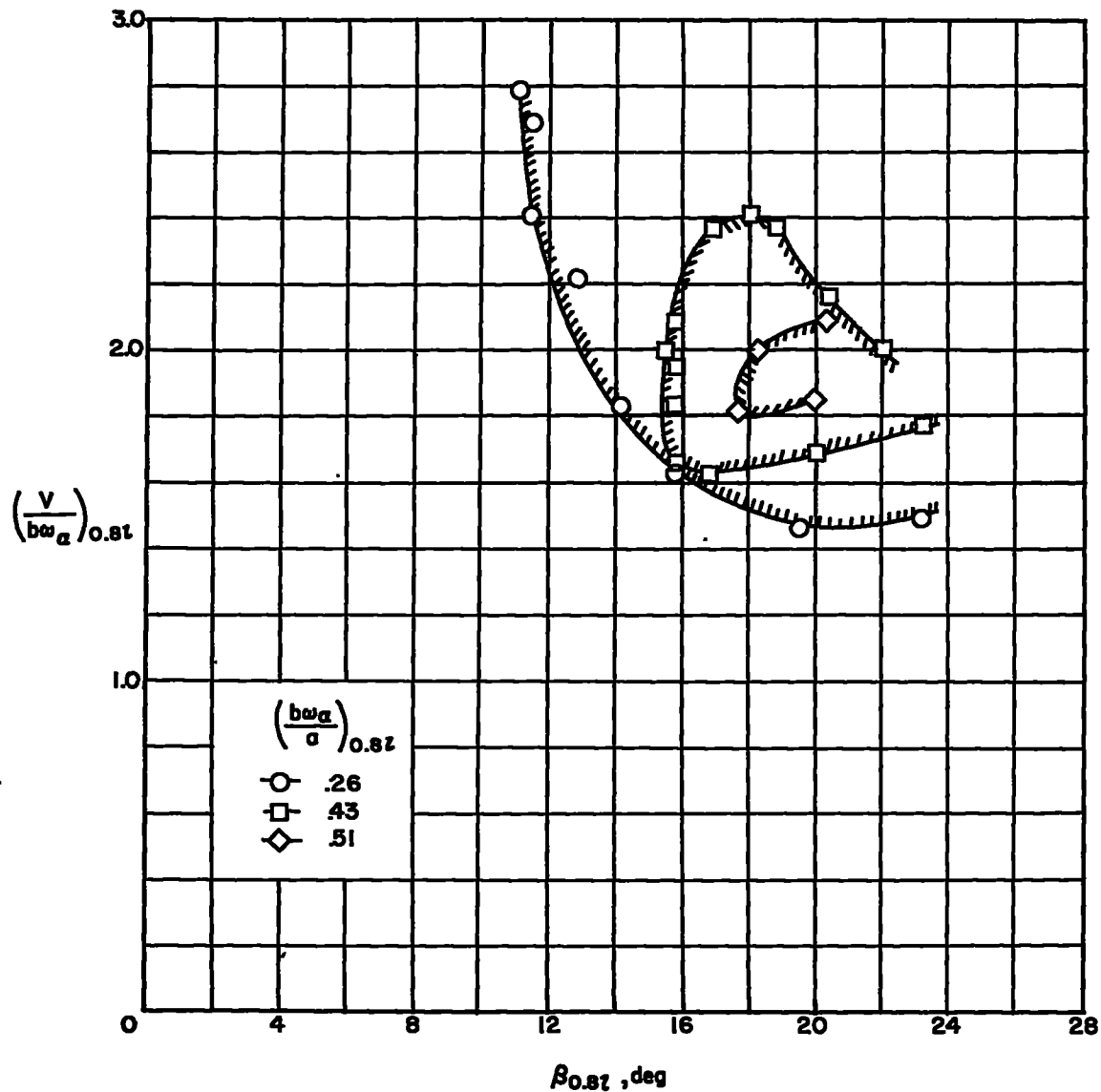


Figure 4.- Flutter-speed coefficient as a function of blade angle for three values of the sound-speed coefficient. Model 2;
 $\rho = 0.00238$ slug/cu ft.

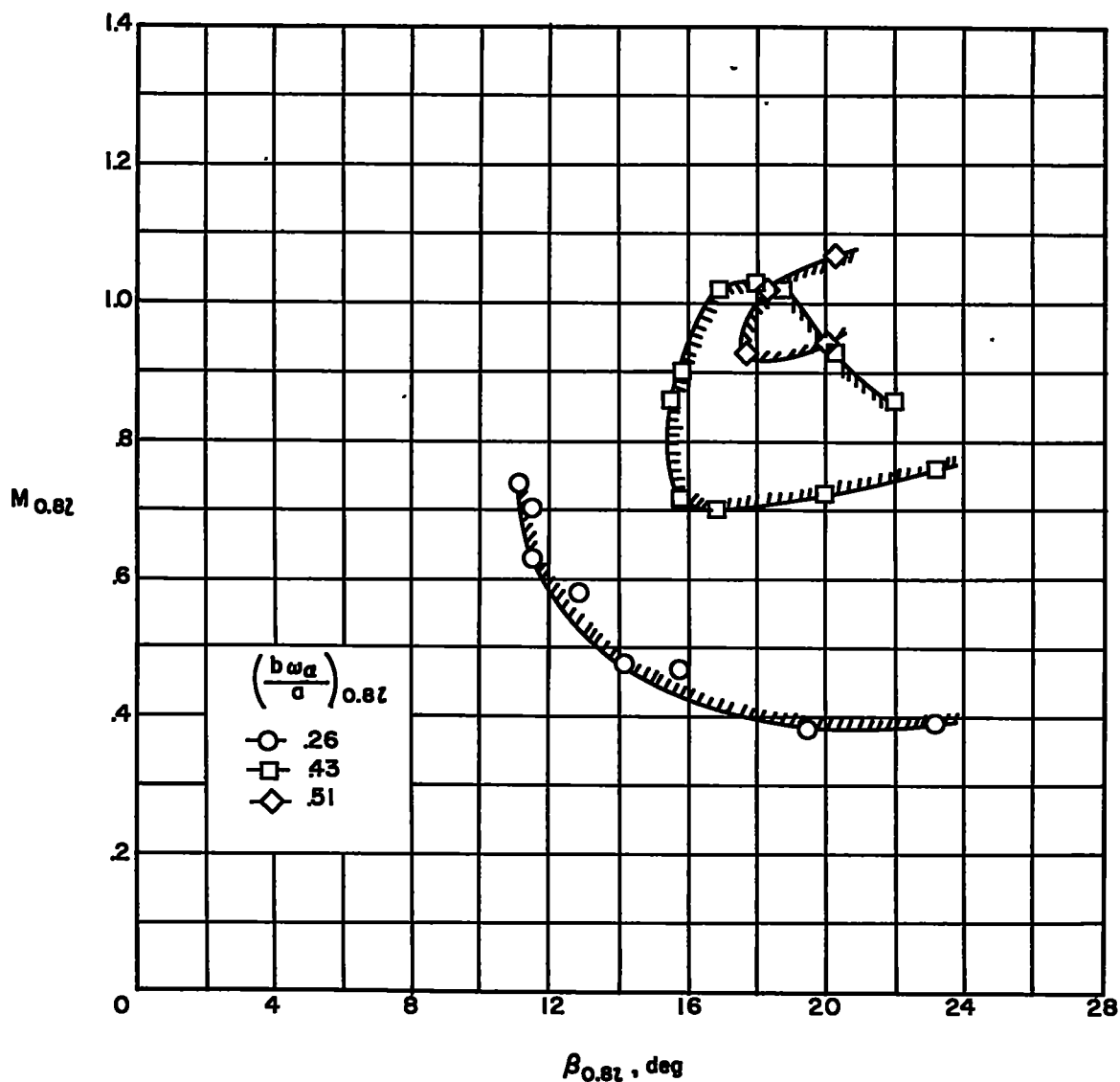


Figure 5.-- Mach number at flutter as a function of blade angle for three values of the sound-speed coefficient. Model 2; $\rho = 0.00238$ slug/cu ft.

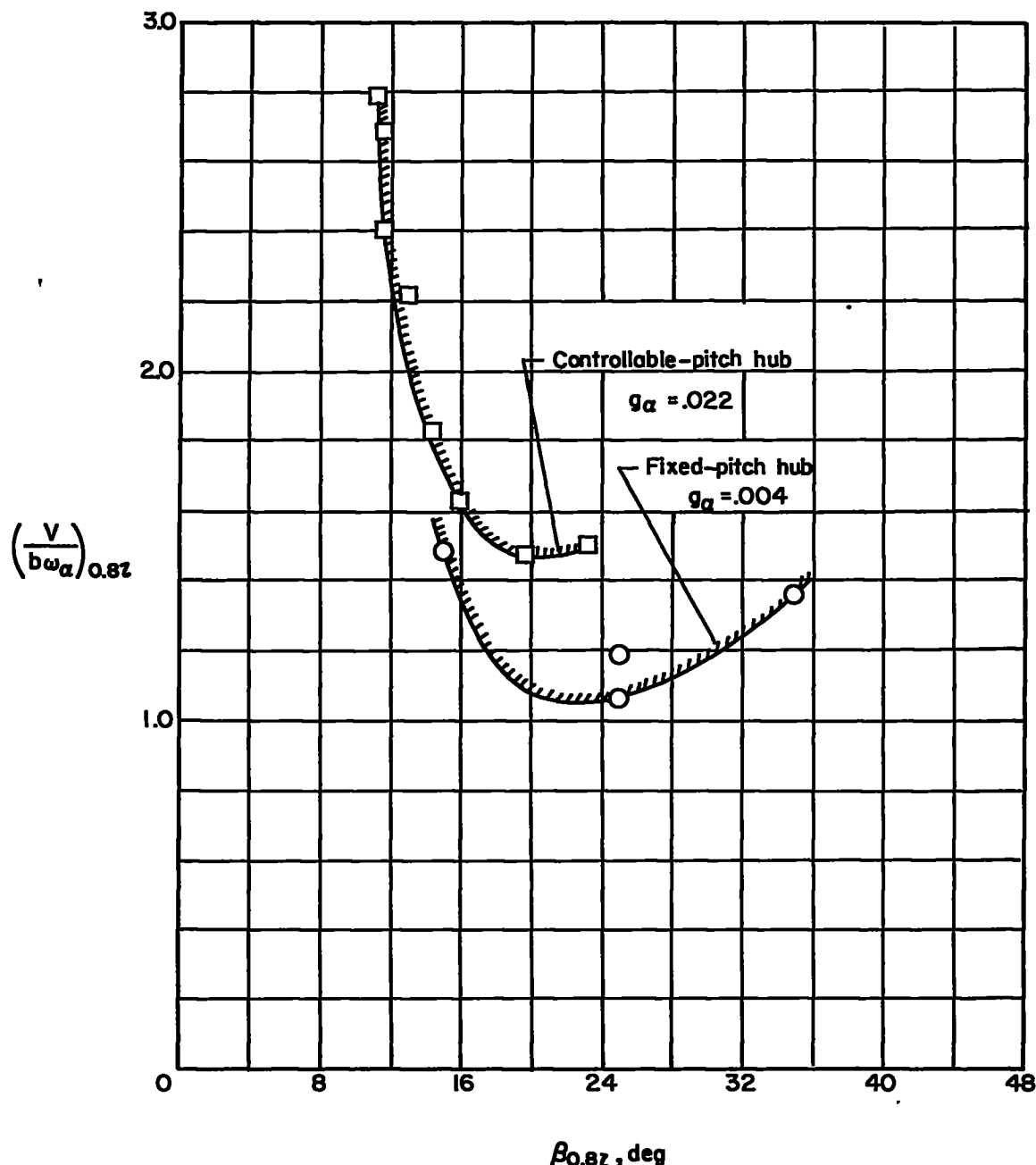


Figure 6.- Flutter-speed coefficient as a function of blade angle for two values of torsional damping coefficient. Model 2;
 $\rho = 0.00238$ slug/cu ft.

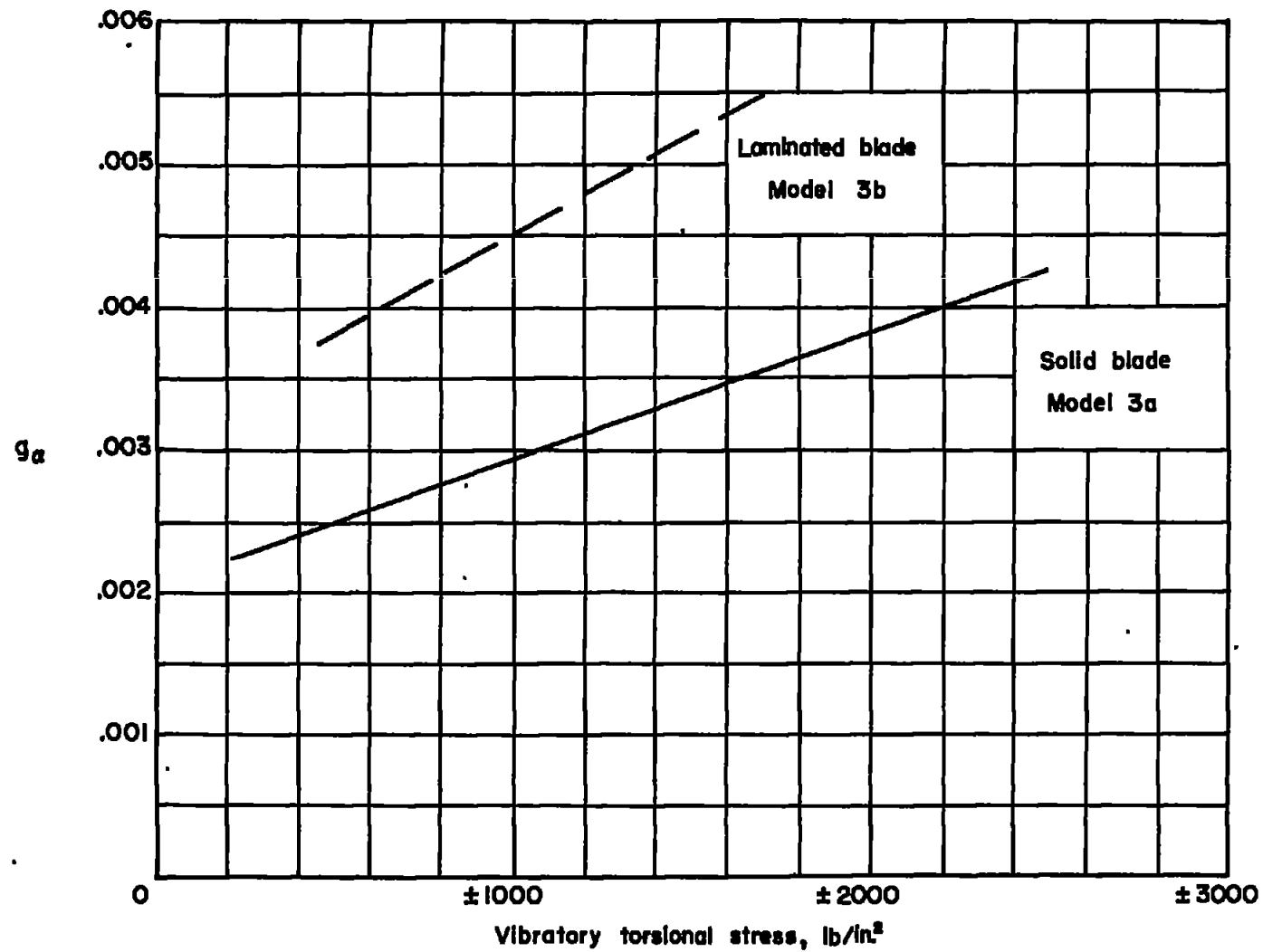


Figure 7.- Variations of torsional damping coefficient as a function of vibratory torsional stress for models 3a and 3b.

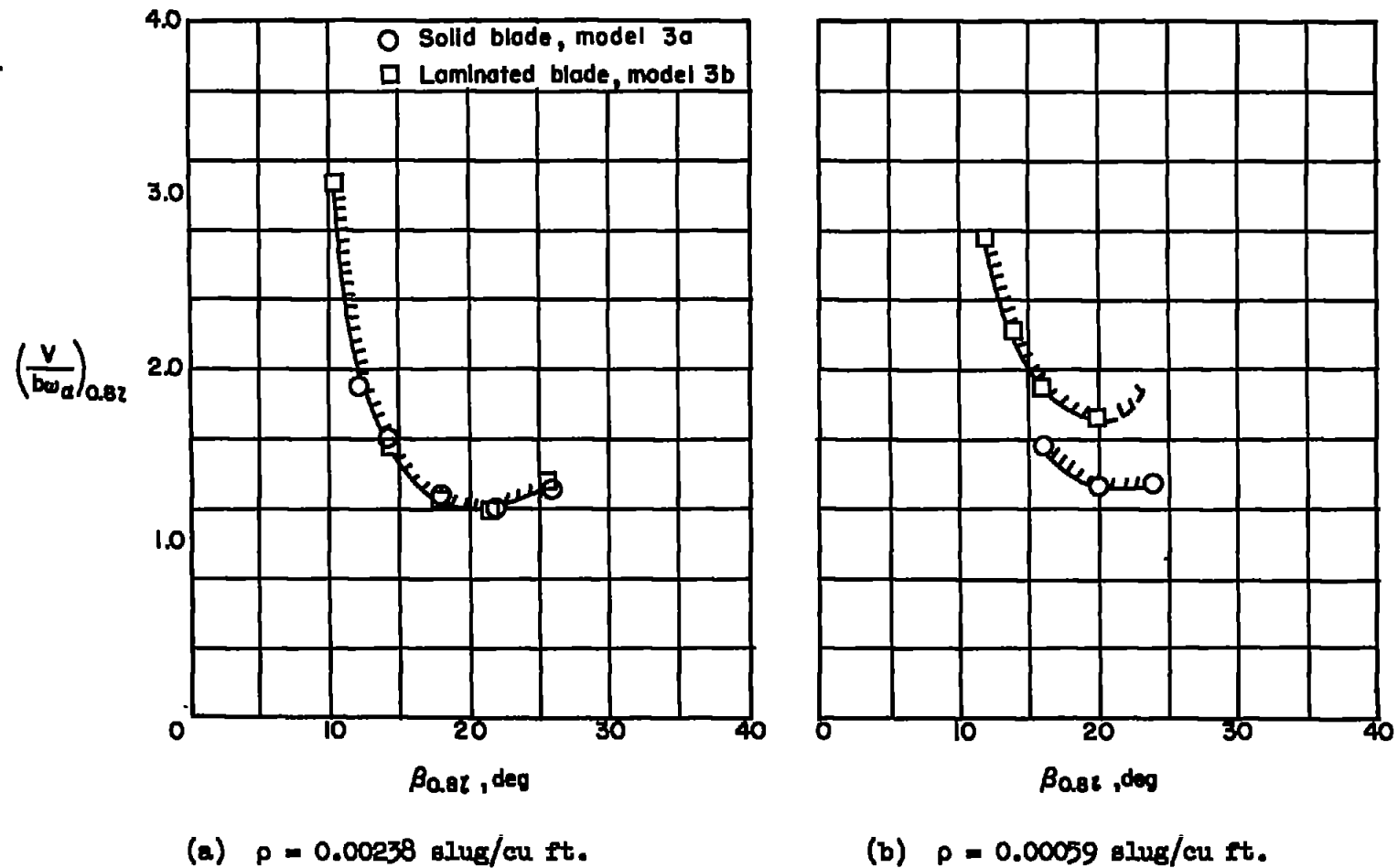


Figure 8.- Flutter-speed coefficient as a function of blade angle for models 3a and 3b.

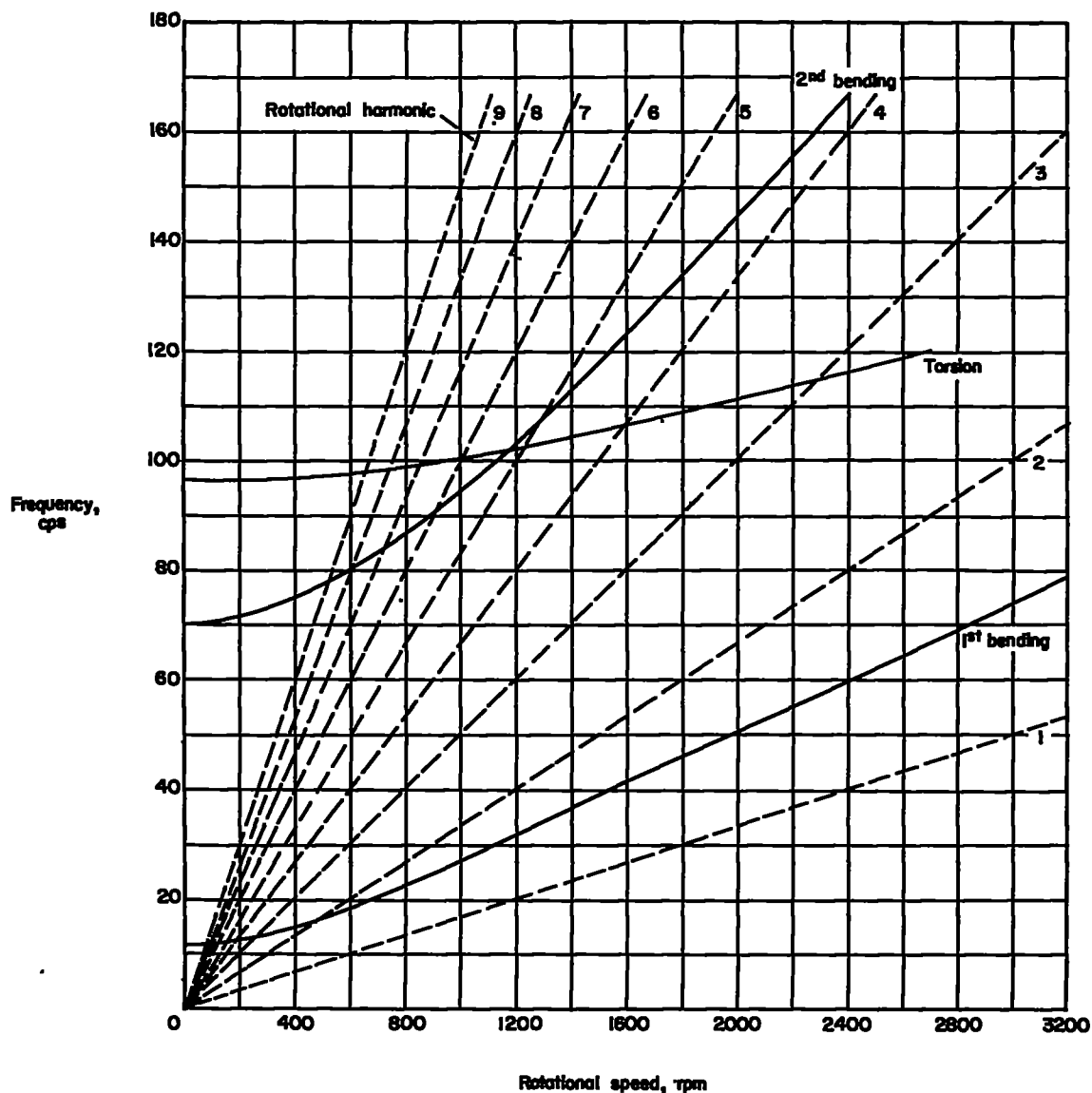
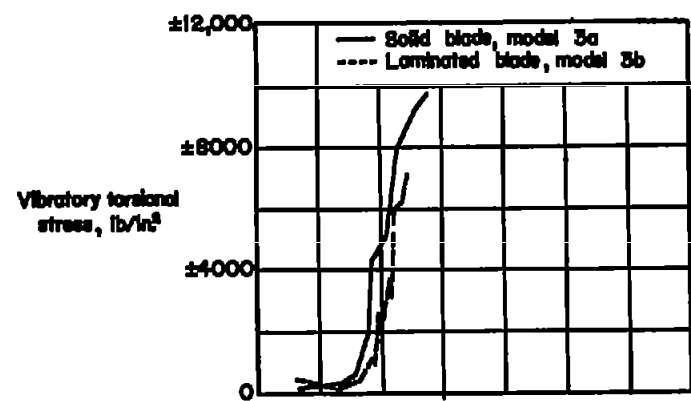
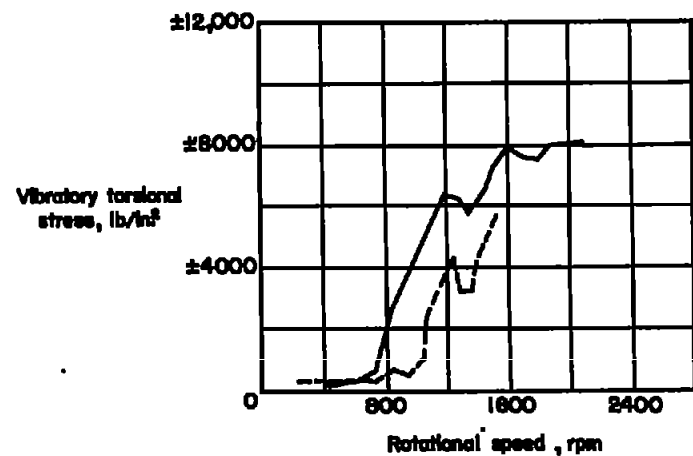


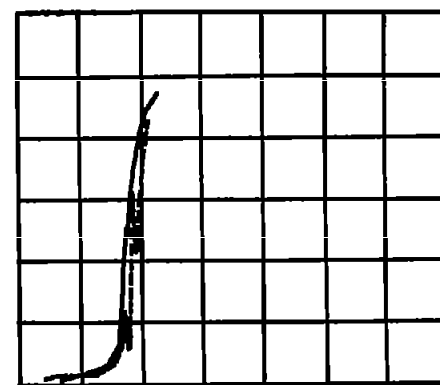
Figure 9.- Frequency spectra for models 3a and 3b.



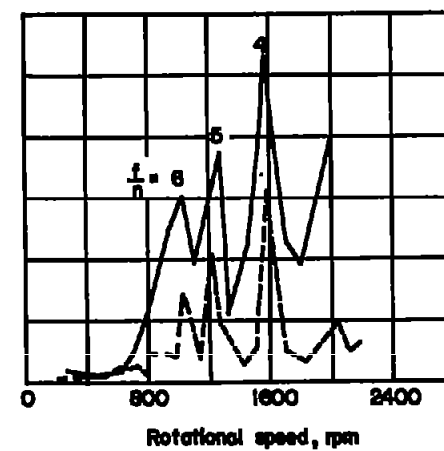
(a) $\rho = 0.00238 \text{ slug/cu ft}$; $\beta = 16^\circ$.



(c) $\rho = 0.00059 \text{ slug/cu ft}$; $\beta = 16^\circ$.



(b) $\rho = 0.00238 \text{ slug/cu ft}$; $\beta = 24^\circ$.



(d) $\rho = 0.00059 \text{ slug/cu ft}$; $\beta = 24^\circ$.

Figure 10.- Vibratory torsional stress as a function of rotational speed for models 3a and 3b.

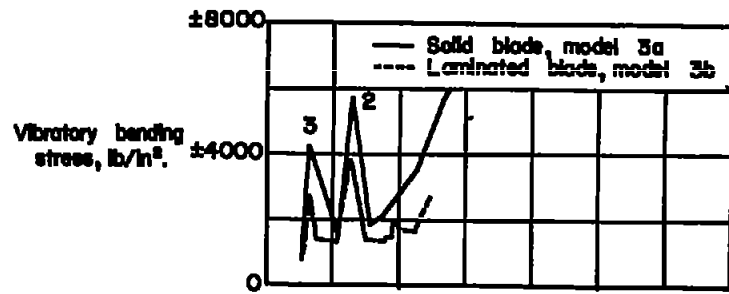
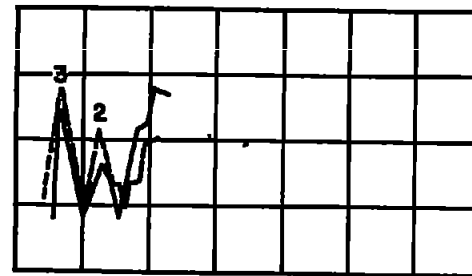
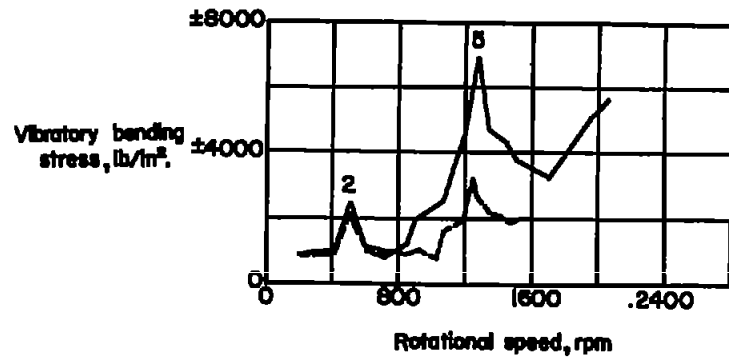
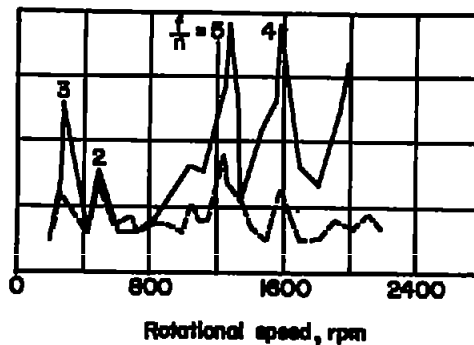
(a) $\rho = 0.00238 \text{ slug/cu ft}$; $\beta = 16^\circ$.(b) $\rho = 0.00238 \text{ slug/cu ft}$; $\beta = 24^\circ$.(c) $\rho = 0.00059 \text{ slug/cu ft}$; $\beta = 16^\circ$.(d) $\rho = 0.00059 \text{ slug/cu ft}$; $\beta = 24^\circ$.

Figure 11.- Vibratory bending stress as a function of rotational speed. Models 3a and 3b.